Nuclear Science and Techniques (2026) 37:32
https://doi.org/10.1007/s41365-025-01847-5

Mass production and performance evaluation of CHSN01 jacket for future fusion applications

Wei-Jun Wang[1,2] · Jing-Gang Qin[1,2] · Yong-Sheng Wu[1] · Jing Jin[1] · Jin-Hao Shi[2] · Yi-Fei Wu[1] · Zheng-Ping Tu[3] · Xiao-Wei Chen[3] · Jian-Gang Li[1,2] · Huan Jin[1]

Received: 3 July 2024 / Revised: 28 August 2024 / Accepted: 9 October 2024 / Published online: 4 January 2026

Abstract

A low-temperature-resistant and high-strength stainless-steel jacket is a key component in the superconducting magnet of a fusion reactor. The development of cryogenic structural materials with high strength and toughness poses a challenge for the future development of high-field superconducting magnets in fusion reactors. The yield strength of the International Thermonuclear Experimental Reactor developed for low-temperature structural materials at 4.2 K is below 1100 MPa, which fails to meet the demand for structural components with yield strengths exceeding 1500 MPa at 4.2 K in the future fusion reactors. CHSN01 (formerly N50H), which is a low-temperature structural material developed in China, exhibits exceptional strength and toughness, thereby making it highly promising for practical applications. Recently, a 30 t jacket measuring approximately 5000 m in total length was produced. Its low-temperature mechanical properties were tested using a sampling method to ensure compliance with application requirements. This paper presents the experimental data of the CHSN01 jacket and tests of the physical properties of the material in the temperature range of 4–300 K. The physical properties were unaffected by magnetic field. Furthermore, this paper discusses the feasibility of employing CHSN01 as a cryogenic structural material capable of withstanding high magnetic fields in next-generation fusion reactors.

Keywords CHSN01 · CICC jacket · Cryogenic steel · Fusion reactor

1 Introduction

Fusion energy represents a clean and sustainable solution to address the global energy crisis, and magnetic confinement tokamak devices offer effective pathways toward the realization of fusion energy development. Notably, the power generated by fusion reactions is directly proportional to the fourth power of the magnetic field strength, thereby emphasizing the pursuit of higher magnetic field strengths. Therefore, future tokamaks such as the current design of the China Fusion Engineering Demo Reactor (CFEDR) [1–3], fusion DEMO reactor (JA DEMO) of Japan [4, 5], European DEMO fusion reactor (EU-DEMO) [6, 7], and SPARC [8] are expected to incorporate high-field superconducting magnets with magnetic fields exceeding 17 T.

A cable-in-conduit conductor (CICC) comprising an inner superconducting cable and outer stainless-steel jacket represents a conventional conductor structure for fusion superconducting magnets, as shown in Fig. 1. During the operation of CICCs, the jacket is filled with liquid helium; therefore, the conductors operate at ultralow temperatures [9]. High magnetic fields generate strong electromagnetic forces that act directly on the structural components of superconducting magnets, such as the CICC jacket [10]. In a limited space, the most effective way to increase the magnetic field strength

This work was supported in part by the National Natural Science Foundation of China (No. 12305196), Anhui Provincial Natural Science Foundation (No. 2308085QA23), Open Fund of Magnetic confinement Fusion Laboratory of Anhui Province (No. 2023AMF03003), and Science Foundation of Institute of Plasma Physics, Chinese Academy of Sciences (No. DSJJ-2024-10).

✉ Huan Jin
jinhuan@ipp.ac.cn

[1] Hefei Institutes of Physical Science, Chinese Academy of Sciences, Hefei 230031, China

[2] Institute of Energy, Hefei Comprehensive National Science Center, Hefei 230031, China

[3] Zhejiang JiuLi Hi-Tech Metals Company Ltd., Huzhou 313012, China

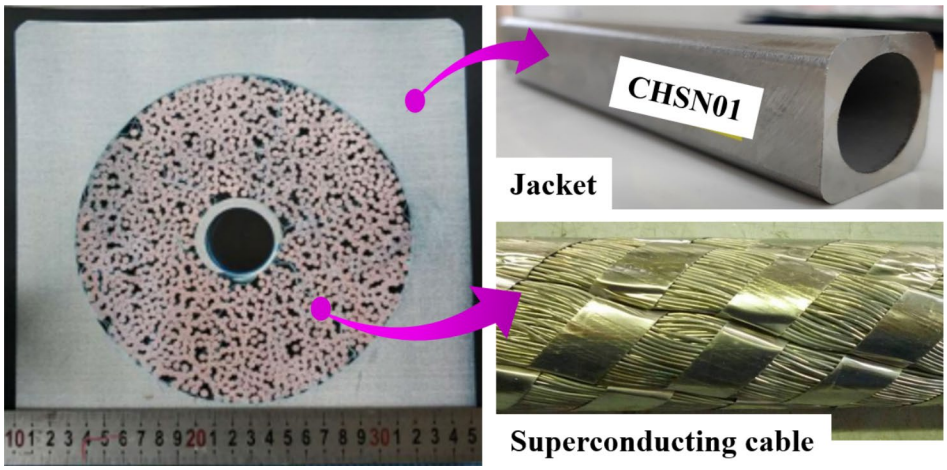

Fig. 1 (Color online) CICC structure diagram

is to increase the current-carrying capacity and current-carrying area of the superconducting cable in a CICC while simultaneously reducing the proportion of structural materials in the CICC. Therefore, the strength of structural materials needs to be urgently improved.

In a CICC, the stainless-steel jacket is required to possess nonmagnetic properties, high strength, exceptional plasticity, and remarkable toughness to operate effectively in a strong magnetic field environment at liquid helium temperature (4.2 K). In the future, the maximum magnetic field strength of the CFEDR will be greater than 17 T, and the maximum operating current of a CICC will be approximately 100 kA. Consequently, the resulting electromagnetic force, which will surpass 1500 kN/m, will directly impact a CICC jacket. According to the current design specifications of the CFEDR, a jacket must have high toughness and plasticity while exhibiting high strength at 4 K. The specific mechanical criteria are as follows. The yield strength (YS) should exceed 1500 MPa, elongation (EL) should exceed 25%, and fracture toughness K_{IC} should exceed 130 MPa · $m^{1/2}$ at 4.2 K [11, 12]. In addition to tensile and fracture toughness, the fatigue crack growth rate (FCGR) must be concurrently characterized.

Currently, the main international materials used for superconducting magnet stainless-steel jackets are low-carbon steel 316LN and 316 L, high-manganese austenitic stainless-steel JK2LB, Incoloy 908, and high-nitrogen austenitic stainless-steel Nitronic 50 (N50) [13]. The structural materials that have been developed for the ITER, such as 316LN and JK2LB, fail to satisfy the requirements of CFEDR applications because of their relatively low yield strength of approximately 1000 MPa at 4.2 K [14–17]. The nominal composition of N50 steel is 22% Cr–13% Ni–5% Mn–0.30% N, and it is a nitrogen-strengthened austenitic stainless steel. N50 steel exhibits nonmagnetic and corrosion-resistant properties along with high strength, thereby rendering it highly promising for applications in low-temperature environments. In the USA, it is referred to as N50, whereas in Japan, it is referred to as XM-19. The N50 material was developed with elevated levels of carbon (maximum of 0.06%) and nitrogen (ranging from 0.2 to 0.4%) to enhance its structural properties.

The traditional N50 material cannot be directly applied to jackets, mainly because it is not resistant to high-temperature aging. The traditional N50 strengthened by high-carbon (0.06% max) and high-nitrogen (0.2–0.4%) contents easily forms a precipitated phase during 650 °C aging. For the composition design of low-temperature steel, minimizing the carbon content and increasing the manganese and nickel contents are crucial for effectively reducing the toughness and brittleness transition temperature. In addition, appropriate amounts of alloying elements, such as niobium, vanadium, and nitrogen, should be considered to generate fine crystals and increase precipitation. These elements not only enhance the steel strength but also improve its plasticity and stability.

A modified N50 alloy was developed in China by completely eliminating δ ferrite and strictly controlling its carbon (maximum 0.01%) and oxygen (maximum 20 ppm) contents. By ensuring that $Ni_{eq}/Cr_{eq} > 1.1$, the presence of high-temperature δ ferrite was effectively eliminated. The precipitation of $M_{23}C_6$ was inhibited by controlling the C content to ≤ 0.01wt.%. By controlling the Nb and V contents, a certain amount of nitride can be retained to refine the grains and improve the comprehensive mechanical properties [18–20]. The addition of trace B can significantly inhibit the nucleation and coarseness of the Cr_2N and Laves phases, which is conducive to improving the toughness and fatigue resistance of the material [21]. Chinese researchers have performed many improvement and optimization studies based on the traditional N50 components. China developed a modified version of the traditional N50 material, named as cryogenic high-strength high-nitrogen steel No. 1 (CHSN01), which replaced the previous N50H model. The

chemical composition of a CHSN01 billet is presented in Table 1.

The production process of the CHSN01 base material includes an electro-slag remelting (ESR) step, which ensures the refinement and cleanliness of the steel microstructures by minimizing nonmetallic inclusions and eliminating exogenous macro-inclusions. Circle-in-square jackets were fabricated by Jiuli Company using a combination of hot extrusion and drawing processes. As of June 2024, a 30 t CHSN01 jacket, with an approximate length of 5000 m, has been manufactured. In this study, the properties of the mass product were evaluated, and the physicochemical properties of the material were studied.

2 Sample preparation and test procedures

2.1 Jacket profile

The CHSN01 material needs to be produced using medium-frequency induction furnace steelmaking, followed by a suitable refining process aimed at minimizing the presence of impurity gases, such as hydrogen and oxygen. To achieve the desired properties, appropriate refining techniques such as vacuum oxygen decarburization and ESR must be employed.

CHSN01 pipes manufactured by Jiuli Company in China undergo a hot extrusion process followed by multiple drawing steps. Subsequently, an intermediate annealing treatment is required before subjecting them to a final solution annealing (SA) at temperatures ranging from 1120 to 1200 °C. The outer and inner hole diameters of a circle-in-square pipe are 37.7 mm and 29.5 m, respectively. A 30 t CHSN01 jacket with a total length of approximately 5000 m has been produced. Mass production of the CHSN01 jacket is shown in Fig. 2. Each batch in the solution furnace is considered as a separate entity, with a total of 20 batches.

The surface roughness of the jackets, as measured by R_a, is below 1.6 µm, whereas the equivalent permeability is below 1.01. In addition, each individual jacket measures at least 9 m in length. The jacket grain size number, as per ASTM standards, exceeds four, and intergranular corrosion is not observed. Furthermore, micrographs at a magnification of 500x reveal the absence of discernible ferrite traces.

During CICC coil manufacturing, the jacket must be compressed (the inside of the jacket is fitted to a cable), bent + straightened + wound (conducive to transportation), and treated to Nb_3Sn superconductor reaction aging [22, 23]. The compaction process uses a cold-rolling machine to reduce the outer dimensions from 37.7 mm × 37.7 mm to 35.1 mm × 35.1 mm, thereby ensuring precise dimensional control. Subsequently, a series of cold-working (CW) operations are performed on the jackets, which result in an overall deformation of approximately 4%. Following this cold-working stage, the Nb_3Sn conductor jackets are annealed in a vacuum furnace. A heat treatment solution specifically designed for ITER Nb_3Sn is used to age the jackets [24, 25]. The duration of the Nb_3Sn superconductor reaction aging treatment cycle is as follows: 210 °C for 50 h + 340 °C for 25 h + 450 °C for 25 h + 575 °C for 100 h + 650 °C for 100 h. During the heat

Table 1 Chemical composition requirement of a CHSN01 billet

Element wt.%	C	Si	Mn	P	S	Cr	Ni	Mo	V	Nb	N	O
CHN01	≤0.01	≤0.3	4.5−6.0	≤0.015	≤0.005	20.5−23	13.5−15.5	1.5−2.5	0.1−0.25	0.06−0.18	0.25−0.35	≤0.002

Fig. 2 (Color online) Mass production of the CHSN01 jacket

treatment process, vacuum is always maintained at approximately 5×10^{-3} Pa.

2.2 Mechanical test samples and procedures

Plate-like tensile samples were obtained by cutting the corner and face of a jacket within the space of limited thickness. The total length of the flaky tensile sample was 67 mm, length of the parallel section was 26 mm, thickness was 3 mm, and original gauge length was 20 mm. Tensile test specimens were fabricated according to the ASTM E1450 guidelines [26]. Compact tension (CT) specimens for fracture toughness testing were prepared with a width (W) of 25 mm and thickness of 3 mm, without any side grooves. These CT specimens adhered to the JIS Z 2284 standard for fracture toughness [27]. FCGR CT specimens with a width of 30.6 mm and thickness of 3 mm were prepared. The dimensions of the FCGR specimens were in accordance with the specifications in ASTM E647 [28]. The direction of crack processing of the fracture toughness and FCGR samples was parallel to the length direction of the jacket. The locations of the test samples are shown in Fig. 3.

The total number of batches was 20, and each batch contained approximately 27 jackets. One jacket was required per batch for sampling purposes, and each batch was tested for two tensile strengths (corner and face), one fracture toughness, and one FCGR strength. The test samples were consistently enclosed within a thermally insulating sleeve and continuously immersed in liquid helium throughout the experiment [29, 30]. A thermometer was placed above a sample to ensure that the sample was adequately cooled, and the temperature was guaranteed to be less than 7 K during the test. The tensile tests were conducted under displacement control at a strain rate below 5×10^{-4} s^{-1}. During the tests, the strain was measured using a clip-on extensometer (Epsilon model 3542-025 M-50-LT) in the range of 10%. The mechanical properties of the samples, including the YS, EL, and ultimate tensile strength (UTS), were determined by testing. Each fracture toughness specimen was precracked at room temperature at a frequency of 3 Hz.

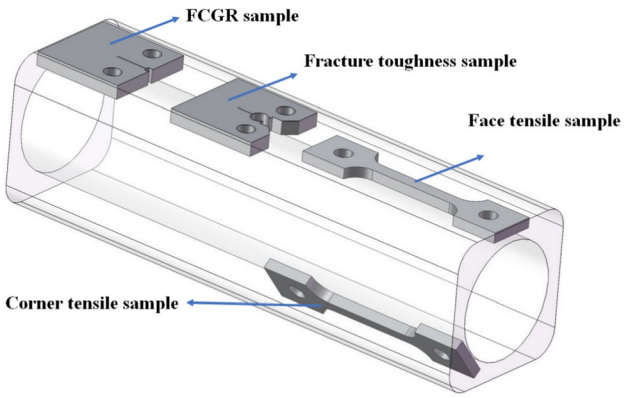

Fig. 3 (Color online) Positions of the test samples for each batch of jacket

2.3 Weld proof samples

In the production process of CICCs, butt welding of the jackets is necessary to ensure a sufficient conductor length. Subsequently, a proof sample (one per machine) is welded using the same machine used for conductor production to assess the welding quality. Tungsten inert gas (TIG) welding technology is used for joint welding, and the shielding gas is a mixture of 70% argon and 30% helium to obtain a fine grain size. The circular area around the inner hole of a jacket is welded using an automatic track welding machine, except for the first line, which is welded by self-fusion. The corners are manually TIG-welded using a 1.6 mm diameter electrode. Refer to the previous development of jacket-welding techniques and welding processes [31].

The quality of the welded joints must be ensured by nondestructive testing, which includes conducting penetration tests, examining X-rays, and performing helium leak tests. Subsequently, the conductor is subjected to necking and extrusion after being pulled through the conduit during the manufacturing of the superconducting cables. Therefore, during the conductor preparation process, subjecting both the jacket and its welded joints to CW and aging procedures is imperative. In this study, five groups of welded joints were prepared, and ten tensile samples of the welded joints were obtained (two tensile samples for each group). The size and test procedure for the tensile samples were the same as those described in Sect. 2.2. According to the requirements of the ITER, the gauge length of the tensile specimen of a welded joint was the sum of twice the thickness of the sample and the width of the weld. The difference was that the original gauge length of the welded joint tensile sample was 10 mm. The YS of the welded joint exceeded 1400 MPa, and the elongation exceeded 20% at 4.2 K.

2.4 Physical property test

To obtain the basic physical properties of the material, we used a physical property measurement system (Quantum Design Inc., DynaCool) to measure the resistivity, specific heat capacity, and thermal conductivity of the CHN01 jacket [32]. A jacket was operated under a strong magnetic field at 4.2 K. The properties of the material were studied at low temperatures and under magnetic fields. Resistivity and thermal expansion test samples with volumes of 8 mm × 2 mm × 2 mm were prepared via wire cutting from the jacket after CW and heat treatment with aging (HT). The resistivity test required ohmic contact between the sample

and electrode. The sample size for testing the specific heat capacity was 2 mm × 1 mm × 1 mm, and the mass was 30.4 mg. The sample was affixed to a mounting platform using a thin layer of Apiezon N grease to precisely measure the specific heat capacity. To ensure accurate results, the heat capacities of the sample platform and grease were also determined [33, 34].

3 Results and discussion

3.1 Mechanical test results

The results, including the YS, EL, and K_{IC}, are shown in Fig. 4. The CHSN01 samples (after undergoing CW + HT) exhibit a YS exceeding 1500 MPa and an elongation greater than 25% under 4.2 K test conditions. Forty tensile samples were tested in twenty batches of jackets. Figure 4a shows that the average YS of the CHSN01 jacket is 1560 MPa, and the standard deviation is 42.2. The average UTS of the CHSN01 jacket is 1828 MPa. The average EL of all the CHSN01 jacket samples is 32.7%, and the standard deviation is 2.4. The strength at the corner position is slightly higher than that at the face position, owing to the uneven force of the jackets during CW. The test results exhibit excellent repeatability and consistency.

The YS shown in Fig. 4b is the average YS of the corner and face positions of each batch of jackets. Twenty fracture toughness samples were tested in twenty batches of jackets. J_{IC} was acquired and transformed into $K_{IC}(J)$ according to the guidelines in JIS Z 2284. The relationship between the YS and fracture toughness $K_{IC}(J)$ of the CHSN01 jacket is shown in Fig. 4b. The average $K_{IC}(J)$ of all CHSN01 jacket samples is 220 MPa · $m^{1/2}$, and the standard deviation is 24.9. The fracture toughness tends to decrease with increasing strength. Noticeably, the fracture toughness of the jackets satisfies the requirement of exceeding 130 MPa · $m^{1/2}$ and has a certain safety margin.

The relationship between the rate of fatigue crack propagation da/dN and range of stress intensity factor ΔK in the Paris regime is shown in Fig. 4c for a CHSN01 jacket operating at 4.2 K. The FCGR of the CHSN01 jacket is lower than that of the CFEDR center solenoid model coil (CSMC) jacket (modified 316LN material). When ΔK is less than 35 MPa · $m^{1/2}$, the ability of the CHSN01 jacket to prevent crack propagation is very strong, i.e., the threshold value of the crack growth of CHSN01 is high, and the 316LN jacket begins to expand.

The fracture morphology of a jacket tensile specimen was characterized using scanning electron microscopy, and the fracture mode was assessed. As depicted in Fig. 5, micrographs of the fracture surface exhibit a characteristic ductile fracture pattern distinguished by numerous dimples. During low-temperature tensile deformation, deformation twins are produced, which increase the work-hardening rate, delay the occurrence of necking, and increase the strength and elongation of CHSN01.

The mechanical properties of the mass produced CHSN01 jacket exhibit good stability. The exceptional strength of the jacket is attributed to work hardening during cold deformation in conjunction with meticulous material design. The mechanical performance test results of all the samples meet the technical requirements of the CFEDR. The CHSN01 jacket has a 40% higher YS, comparable plasticity and toughness, and better fatigue resistance compared with a 316LN jacket. The CHSN01 jacket for a CICC meets the requirements of future fusion reactor applications and has great potential. The jacket has high strength, toughness, and plasticity, which are the basis for the safe operation of future devices.

3.2 Welding test result

The welding test results, including the YS and EL, are shown in Fig. 6. The welded joint samples of a CHSN01 jacket (after undergoing CW + HT) exhibit a YS exceeding 1400 MPa and an EL exceeding 20% under 4.2 K test conditions. Ten tensile samples were tested. Figure 6 shows that the average YS of the CHSN01 jacket welded joints is 1445 MPa, and the standard deviation is 45. The average EL of all the CHSN01 jacket welded joint samples is 22.3%, and the standard deviation is 3.1. The strength of a welded joint is 93% of that of the base material. Currently, the preparation of Nb_3Sn CICC conductors is predominantly simulated, and the stability of the welding joint performance has been observed. The consistency of the welded joint performance is an important index to prove the welding quality and evaluate the application of the jacket mass.

3.3 Physical property test results

Figure 7 shows the thermal expansion ($\Delta L/L$) of CHSN01 steel from 4 to 300 K. Thermal contraction primarily occurs within the temperature range of 300 K– 100 K, exhibiting minimal thermal shrinkage below 50 K owing to the absence of lattice vibrations. The thermal shrinkage behaviors of CHSN01 and 316LN become nonlinear at low temperatures and tend toward linearity as the temperature is elevated to ambient conditions. The thermal contraction of the 316LN jacket between 300 K and 4 K is approximately 0.3117%, whereas that of the CHSN01 jacket is approximately 0.2726%, indicating a smaller magnitude than that of the former [35]. The thermal contraction of the Nb_3Sn wire between 300 K and 4 K is approximately 0.21% [36]. The shrinkage coefficient of the material is mainly related to its Ni–Cr equivalent ratio. The Ni_{eq}/Cr_{eq} ratio of CHSN01 is

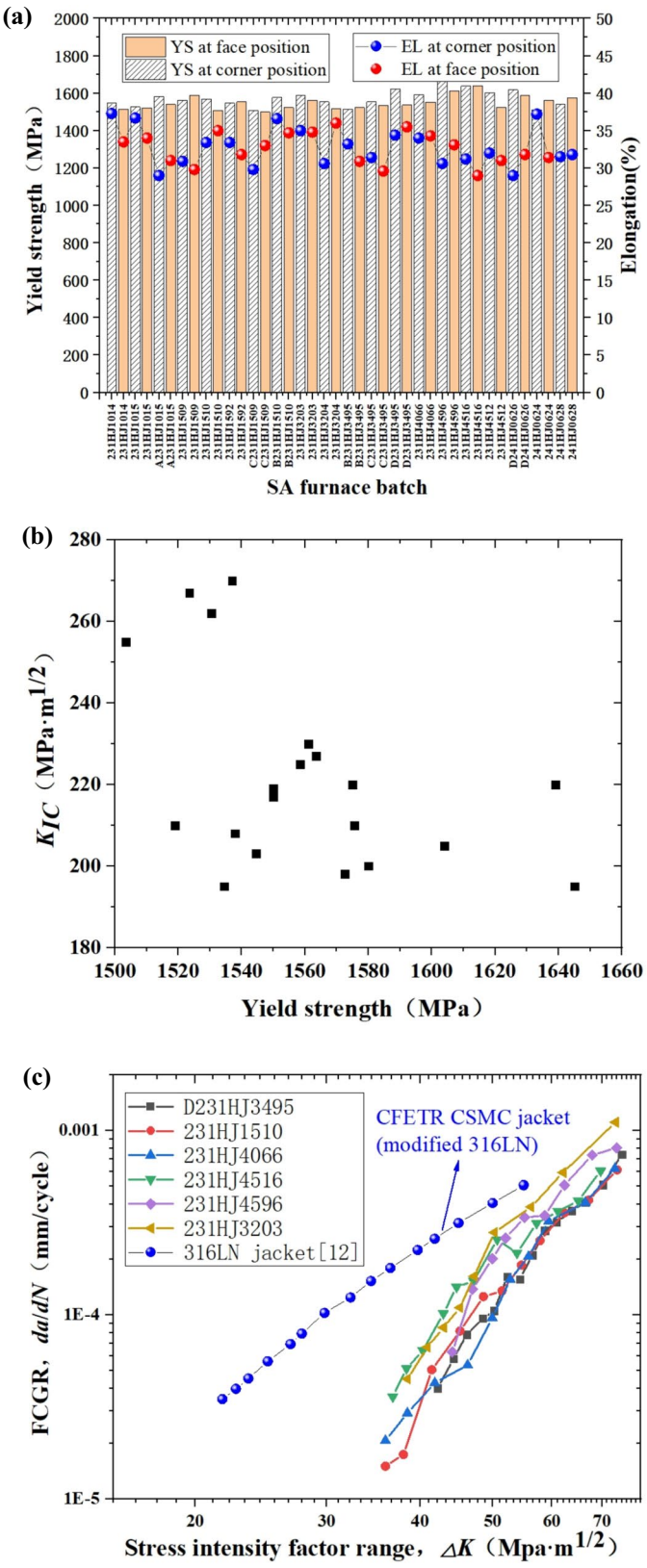

Fig. 4 (Color online) Jacket mechanics test results at 4.2 K. (**a**) The yield strength and elongation of the samples. (**b**) The yield strength and K_{IC} of the samples. (**c**) Test curve of the FCGR. All the curves are for CHSN01 except that of the center solenoid model coil (CSMC), and the serial numbers represent different furnace batches in the legend

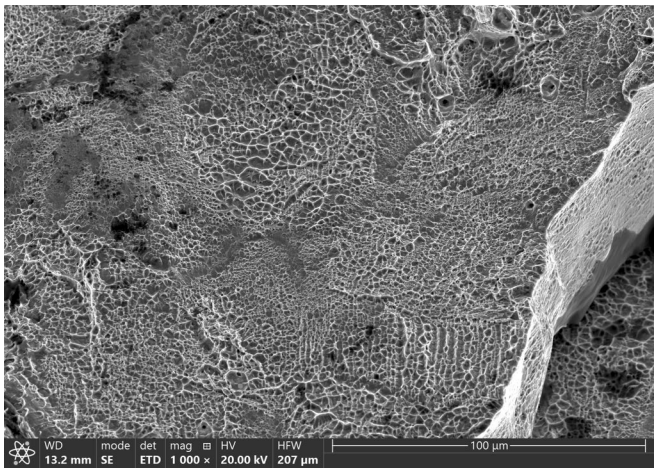

Fig. 5 (Color online) Fracture morphology of a jacket tensile specimen

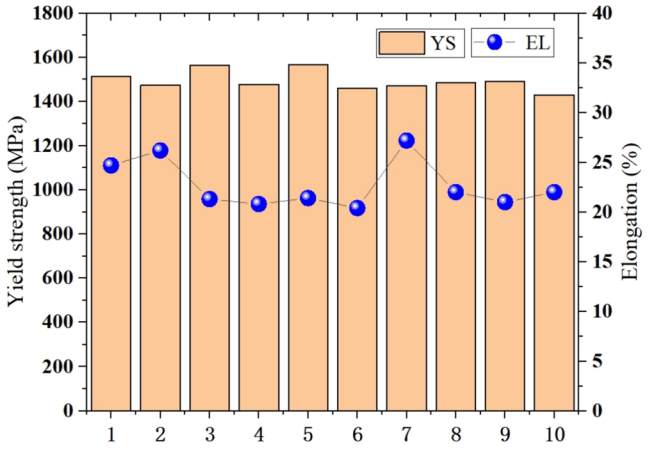

Fig. 6 (Color online) Mechanics test results at 4.2 K of the welded joints of a jacket

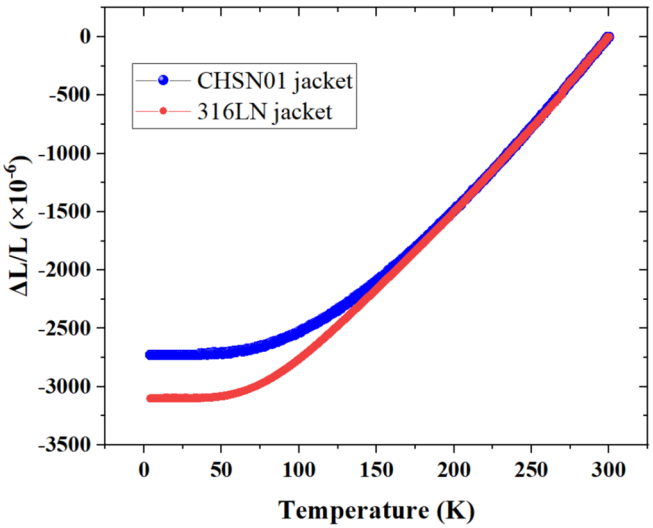

Fig. 7 (Color online) The thermal expansion of the CHN01 jacket from 4 to 300 K

higher than that of 316LN. In general, the larger the Ni–Cr equivalent ratio, the smaller the thermal shrinkage of the material. For the CICC conductor structure, the thermal shrinkage coefficients of the jacket and superconducting materials are approximately the same, which prevent the influence of thermal stress on the superconducting material. A low coefficient of thermal expansion is more suitable for Nb_3Sn CICC jackets, which can effectively reduce the

influence of the thermal shrinkage stress on the performance of superconducting cables.

Figure 8a shows the resistivity of CHSN01 steel from 4 to 300 K. Figure 8b shows the relationship between the resistivity and magnetic field of CHSN01 steel at 4.2 K. Two magnetic fields parallel and perpendicular to the sample were tested.

The CHSN01 jacket resistivity is $6.7 \times 10^{-7}\Omega$·m at 4.2 K. The resistivity of the CHSN01 jacket decreases gradually with decreasing temperature, and the trend is similar to that of the 316LN jacket. Both CHSN01 and 316LN are austenitic stainless steels and exhibit negligible differences in resistivity.

The background magnetic field strength increases from 0 to 12 T, and the resistivity of the material does not change significantly. The resistivity of the CHSN01 jacket does not change significantly under a strong magnetic field. No new substances are produced in the steel under extremely low temperatures and strong magnetic fields. The resistivity of the material is not affected by the strength of the magnetic field; therefore, it is suitable for applications in high magnetic field devices.

The specific heat capacity of the CHSN01 jacket without a magnetic field and with a backfield strength of 10 T was tested; the test results are shown in Fig. 9. A strong correlation exists between the specific heat capacity and temperature. Similar to most metallic materials, the specific heat capacity decreases with decreasing temperature. In the temperature range from 50 to 4 K, the slope of the curve gradually decreases, thereby indicating that the rate of change of specific heat capacity with temperature decreases. The test curves with and without background magnetic field coincide. The specific heat capacity of the CHSN01 material is not affected by the magnetic field. At 4 K, the CHSN01 material specific heat capacity is $2.0\,\mathrm{J/(kg \cdot K)}$.

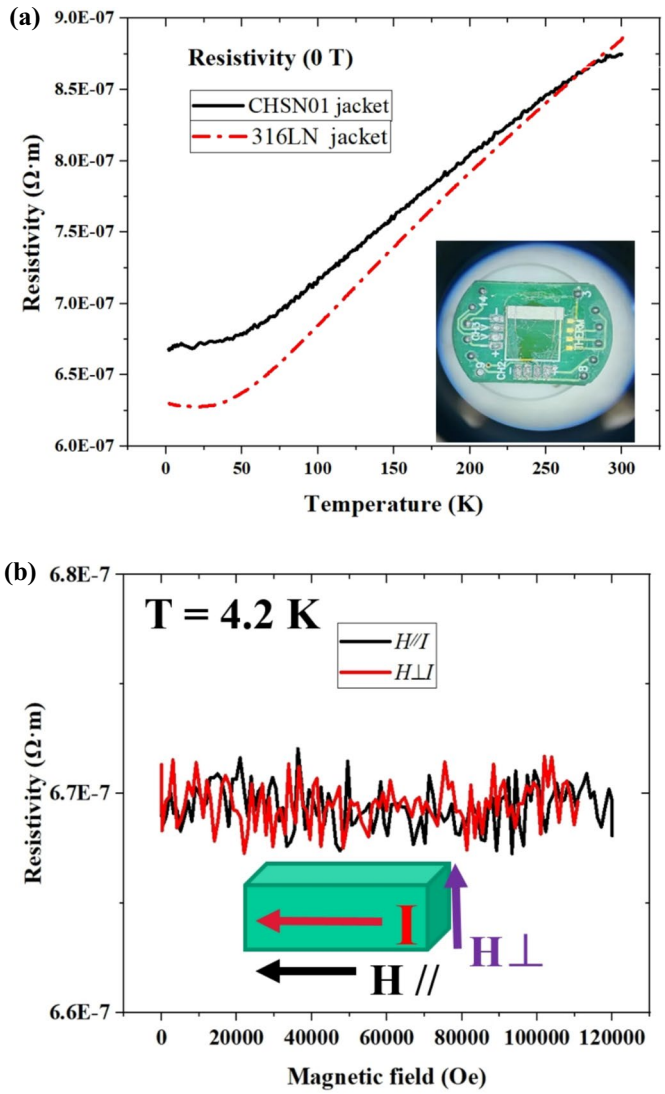

Fig. 8 (Color online) Resistivity test curve of the CHSN01 jacket. **a** The relationship between resistivity and temperature. **b** The relationship between resistivity and magnetic field

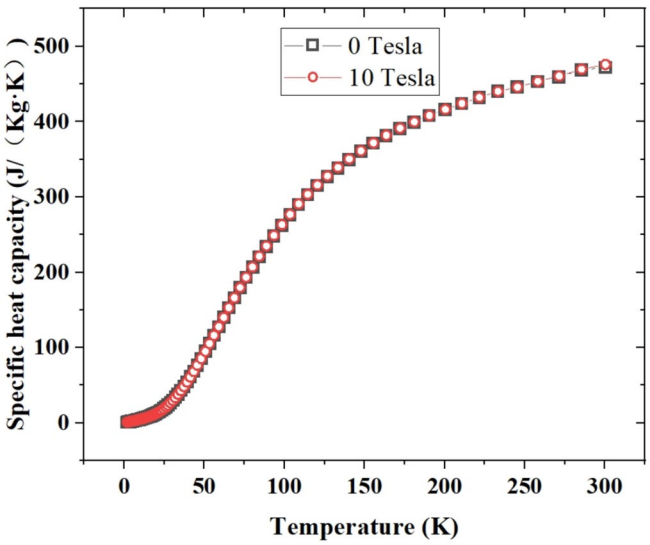

Fig. 9 (Color online) The relation of the specific heat capacity with temperature

Figure 10 shows the relationship between the thermal conductivity and temperature of the CHSN01 material. In the temperature range of 350 K–100 K, the thermal conductivity decreases with decreasing temperature, but the decrease is not large. Thermal conductivity tests were conducted at the Institute of Solid-State Physics, Chinese Academy of Sciences. The obtained results for the thermal conductivity without a background magnetic field are in substantial agreement with those previously reported by the Technical Institute of Physics and Chemistry [33]. The thermal conductivity of CHSN01 is not affected by the magnetic field.

For the design of CICC superconducting magnets, the resistivity, specific heat capacity, and thermal conductivity of the jacket are the key input parameters. Comprehensive testing of the physical properties of a CHSN01 jacket, including resistivity, thermal shrinkage coefficient, specific heat capacity, and thermal conductivity, was performed over a temperature range from 4 to 300 K. Remarkably, the magnetic field had no discernible impact on these physical properties, thereby rendering the material suitable for deployment in environments characterized by low temperatures and strong magnetic fields. Fundamental data pertaining to the physical properties of CHSN01 can serve as valuable reference information for its application in low-temperature research.

4 Summary

(1) China has prepared a 30 t CHSN01 jacket measuring approximately 5000 m in total length and shown the capability for mass production. The domestically developed CHSN01 material from China exhibits

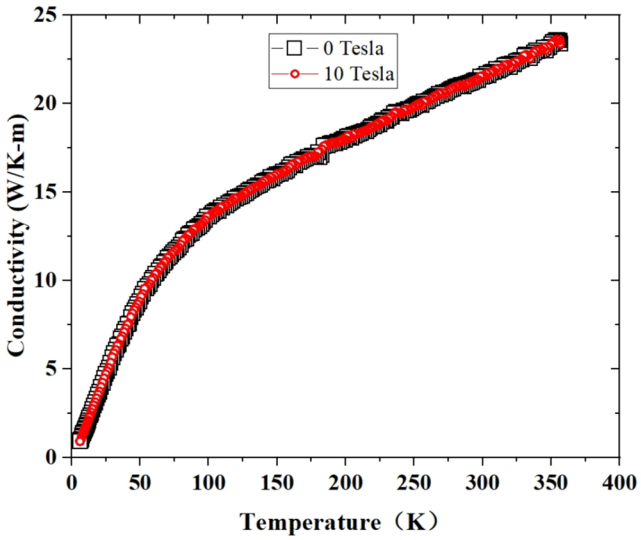

Fig. 10 (Color online) The relation of thermal conductivity with temperature

exceptional mechanical properties at 4.2 K and has been effectively utilized to fabricate CICC jackets. These CHSN01 jackets for CICC applications not only satisfy the stringent requirements of future fusion reactor implementations but also exhibit tremendous potential for various other practical applications.

(2) Low-temperature mechanical properties of the CHSN01 jacket were assessed using a sampling methodology. At 4.2 K, the average YS of the CHSN01 jacket was 1560 MPa, average EL was 32.7%, and average $K_{IC}(J)$ was 220 MPa · $m^{1/2}$. The CHSN01 jacket exhibited better fatigue resistance than a 316LN jacket. The YS of the CHSN01 jacket was enhanced by 40% compared to that of the 316LN jacket, whereas the plasticity and toughness remained comparable. CHSN01 jacket welded joint samples exhibited exceptional mechanical properties with a YS exceeding 1400 MPa and an EL greater than 20% under the test conditions at 4.2 K. The strength of a welded joint was 93% of that of the base material.

(3) Large-scale cryoengineering projects such as future interplanetary high-speed flight stainless-steel thin-wall storage tanks, magnetic confinement nuclear fusion, and hydrogen energy have a significant demand for stainless steel with exceptional strength and toughness at temperatures below 20 K. The CHSN01 material possesses the advantages of nonmagnetism, high strength, and high toughness, thereby rendering it suitable for applications in the field of superconducting magnets. The high strength of CHSN01 enables the fabrication of cryogenic structural components with reduced thickness and weight. Furthermore, it can serve as a substitute for 316LN in processes involving liquid hydrogen and oxygen.

Author contributions All authors contributed to the study conception and design. Material preparation, data collection, and analysis were performed by Wei-Jun Wang, Jing-Gang Qin, Yong-Sheng Wu, Jing Jin, Jin-Hao Shi, Yi-Fei Wu, Zheng-Ping Tu, Xiao-Wei Chen, Jian-Gang Li, and Huan Jin. The first draft of the manuscript was written by Wei-jun Wang, and all authors commented on the previous versions of the manuscript. All authors read and approved the final manuscript.

Data availability The data that support the findings of this study are openly available in Science Data Bank at https://cstr.cn/31253.11.sciencedb.j00186.00803 and https://www.doi.org/10.57760/sciencedb.j00186.00803.

Declarations

Conflict of interest The authors declare that they have no conflict of interest.

References

1. Y.T. Song, J.G. Li, Y.X. Wan et al., Engineering design of the CFETR machine. Fusion Eng. Des. **183**, 113247 (2022). https://doi.org/10.1016/j.fusengdes.2022.113247
2. W.J. Wang, Y.S. Wu, J. Jin et al., Structure optimization and performance evaluation of CS CICC jacket based on N50H austenitic steel for future fusion reactor. Cryogenics **139**, 103836 (2024). https://doi.org/10.1016/j.cryogenics.2024.103836
3. Y.D. Lu, J.X. Zheng, X.F. Liu et al., An improved analysis method for assessing the nuclear-heating impact on the stability of toroidal field magnets in fusion reactors. Nucl. Sci. Tech. **35**, 96 (2024). https://doi.org/10.1007/s41365-024-01459-5
4. A. Nishimura, Y. Ono, O. Umezawa et al., Study on development policy for new cryogenic structural material for superconducting magnet of fusion reactor. Nucl. Mater. Energy **30**, 101125 (2022). https://doi.org/10.1016/j.nme.2022.101125
5. K. Tobita, H. Utoh, R. Hiwatari et al., Conceptual design of Japan's fusion DEMO reactor (JADEMO) and superconducting coil issues. J. Phys: Conf. Ser. **1293**, 012078 (2019). https://doi.org/10.1088/1742-6596/1293/1/012078
6. M. Siccinio, J.P. Graves, R. Kembleton et al., Development of the plasma scenario for EU-DEMO: status and plans. Fusion Eng. Des. **176**, 113047 (2022). https://doi.org/10.1016/j.fusengdes.2022.113047
7. R. Kembleton, J. Morris, M. Siccinio et al., EU-DEMO design space exploration and design drivers. Fusion Eng. Des. **178**, 113080 (2022). https://doi.org/10.1016/j.2022.113080
8. Z.S. Hartwig, R.F. Vieira, D. Dunn et al., The SPARC toroidal field model coil program. IEEE T. Appl. Supercon. **34**, 0600316 (2024). https://doi.org/10.1109/TASC.2023.3332613
9. W. Zhou, X. Fang, J. Fang et al., Numerical and experimental analysis of ac loss for CFETR CS model coil. Nucl. Sci. Tech. **28**, 142 (2017). https://doi.org/10.1007/s41365-017-0301-0
10. G. Romano, A. Vostner, D. Bessette et al., Mechanical properties of ITER coil CICC steel jackets production. IEEE T. Appl. Supercond. **26**, 4 (2016). https://doi.org/10.1109/TASC.2016.2537919
11. W.J. Wang, C.Y. Zhao, H. Jin et al., Mechanical properties evaluation of ReBCO CICC jacket based on super-austenitic stainless steel for CFETR high-field magnet. Nucl. Mater. Energy **34**, 101344 (2022). https://doi.org/10.1016/j.2022.101344
12. C.Y. Zhao, W.J. Wang, H. Jin et al., Research on CICC jacket material for high field magnet application. IEEE T. Appl. Supercon. **32**(6), 1–5 (2022). https://doi.org/10.1109/TASC.2022.3163361
13. W.J. Wang, C.Y. Zhao, J. Jin et al., The research on high-strength CICC jackets with YS>1500 MPa at 4.2 K for future fusion applications. Nucl. Mater. Energy **36**, 101474 (2023). https://doi.org/10.1016/j.nme.2023.101474
14. W.J. Wang, Y.F. Wu, Z.P. Tu et al., Evaluation of the mechanical properties of CICC jacket for CFETR superconducting magnet. Fusion Eng. Des. **192**, 113656 (2023). https://doi.org/10.1016/j.fusengdes.2023.113656
15. J. Qin, Y. Wu, K.P. Weiss et al., Mechanical test on the ITER TF jacket. Cryogenics **52**, 336–339 (2012). https://doi.org/10.1016/j.cryogenics.2012.02.003
16. J.G. Qin, K.P. Weiss, Y. Wu et al., Fatigue tests on the ITER PF jacket. Cryogenics **52**, 486–490 (2012). https://doi.org/10.1016/j.cryogenics.2012.05.018
17. J.G. Qin, C. Dai, G.J. Liao et al., Tensile test of SS 316LN jacket with different conditions. Cryogenics **64**, 16–20 (2014). https://doi.org/10.1016/j.2014.08.003
18. R.Z. Zhai, H.L. Zhang, B. Xu et al., Elimination of δ ferrite in N50 steel and its effect on cryogenic mechanical properties. Cryogenics **126**, 103522 (2022). https://doi.org/10.1016/j.2022.103522

19. R.Z. Zhai, H.L. Zhang, S. Liu et al., Influence of carbon content on the microstructure and cryogenic tensile properties of N50 austenitic stainless steel after aging treatment. J. Nucl. Mater. **571**, 154023 (2022). https://doi.org/10.1016/j.2022.154023
20. R.Z. Zhai, H.L. Zhang, X.L. Qi et al., Fabrication and performance evaluation of CICC jacket based on modified N50 austenitic steel for CFETR magnet. J. Mater. Res. Technol. **28**, 3435–3448 (2024). https://doi.org/10.1016/j.2023.12.278
21. R.Z. Zhai, H.L. Zhang, S.L. Pan et al., Effect of boron addition on the microstructure and cryogenic mechanical properties of N50 stainless steel after aging treatment. Mat. Sci. Eng. A-Struct. **881**, 145372 (2023). https://doi.org/10.1016/j.2023.145372
22. H. Ozeki, T. Saito, K. Kawano et al., Effect of change of aging heat treatment pattern on the JK2LB jacket for the ITER central solenoid. Phys. Procedia **67**, 1010–1015 (2015). https://doi.org/10.1016/j.2015.06.190
23. H. Jin, Y. Wu, J. Qin et al., Effect of cold working and aging treatment on mechanical performance of SS316LN tube. Fusion Sci. Technol. **74**(3), 211–218 (2018). https://doi.org/10.1080/15361055.2017.1421365
24. W.J. Wang, M. Yu, J.G. Qin et al., Heat treatment for Nb_3Sn coils of CFETR CSMC. J. Supercond. Nov. Magn. **33**(9), 2663–2668 (2020). https://doi.org/10.1007/s10948-020-05526-x
25. W.J. Wang, J.G. Qin, M. Yu et al., Heat transfer analysis during heat treatment of Nb_3Sn coils for the CFETR CSMC. Fusion Eng. Des. **165**, 112248 (2021). https://doi.org/10.1016/j.2021.112248
26. Standard test method for tension testing of structural alloys in liquid helium. ASTM E 1450 (2016). https://store.astm.org/e1450-16.html
27. Method of elastic-plastic fracture toughness JIC testing for metallic materials in liquid helium. JIS Z 2284 (1998). https://www.jisc.go.jp/app/jis/general/GnrJISNumberNameSearchList?toGnrJISStandardDetailList
28. Standard test method for measurement of fatigue crack growth rates, ASTM E647 (2008). https://store.astm.org/e0647-08.html
29. J.J. Xin, H.C. Zhang, W.J. Sun et al., Microstructure evolution of austenitic stainless steels under high-cycle-fatigue loading at deep cryogenic temperature. Scripta Mater. **226**, 115223 (2023). https://doi.org/10.1016/j.scriptamat.2022.115223
30. J.J. Xin, H.C. Zhang, B.K. Lyu et al., Mechanical performance and deformation mechanisms of ultrastrong yield strength Fe-Cr-Ni-Mn-N austenitic stainless steel at 4.2 Kelvin. J. Mater. Sci. Technol. **189**, 191–202 (2024). https://doi.org/10.1016/j.jmst.2023.12.027
31. W.J. Wang, J. Jin, L. Wu et al., Study on the welding properties of modified N50 CICC jacket for future fusion applications. J. Mater. Res. Technol. **27**, 6094–6103 (2023). https://doi.org/10.1016/j.jmrt.2023.11.076
32. P.F. Rosen, B.F. Woodfield, Standard methods for heat capacity measurements on a quantum design physical property measurement system. J. Chem. Thermodyn. **141**, 103827 (2024). https://doi.org/10.1016/j.cryogenics.2024.103827
33. W. Schnelle, J. Engelhardt, E. Gmelin, Specific heat capacity of Apiezon N high vacuum grease and of Duran borosilicate glass. Cryogenics **39**, 271–275 (1999). https://doi.org/10.1016/S0011-2275(99)00035-1
34. Y. Huang, W. Sun, C. Huang et al., Mechanical and physical properties of modified N50 steel at cryogenic temperatures. Cryogenics **139**, 103827 (2024). https://doi.org/10.1016/j.2024.103827
35. Y. Ozaki, O. Furukimi, S. Kakihara et al., Development of non-magnetic high manganese cryogenic steel for the construction of LHC project's superconducting magnet. IEEE Trans. Appl. Supercond. **12**, 1248–1251 (2022). https://doi.org/10.1109/TASC.2002.1018628
36. A.F. Clark, G. Fujii, M.A. Ranney, The thermal expansion of several materials for superconducting magnets. IEEE Trans. Magn. **17**, 2316–2319 (2003). https://doi.org/10.1109/TMAG.1981.1061462